J. Fluid Mech. (1973), *vol.* 61, *part* 2, *pp.* 219–243
Printed in Great Britain

Instability, coalescence and fission of finite-area vortex structures

By J. P. CHRISTIANSEN
UKAEA Culham Laboratory, Abingdon, Berkshire

AND N. J. ZABUSKY
Bell Laboratories, Whippany, N.J. 07981

(Received 20 September 1972 and in revised form 17 May 1973)

We have made computational experiments to study the stability and long-time evolution of two-dimensional wakes. We have used the VORTEX code, a finite-difference realization of two-dimensional motions in incompressible inviscid fluids. In the first experiment an initial shear-unstable triangular velocity profile evolves into a non-homogeneous, finite-area, asymmetric vortex array and like-signed regions attract and *fuse* (or coalesce). Enhanced transport across the profile is due to 'capture' and convection of small-scale vortex regions by larger opposite-signed vortex regions. In the following experiments we study the stability of an asymmetric four-vortex *finite-area* system corresponding to a von Kármán street of point vortices. Here the critical parameter is b/a, the initial transverse-to-longitudinal separation ratio of vortex centres. At

$$b/a = 0{\cdot}281$$

the four-vortex system is stable and we observe that large-area vortex regions develop elliptical ($m = 2$), triangular ($m = 3$), etc. surface modes owing to mutual interactions. At $b/a = 0$ the measured growth rate is smaller than that for the corresponding von Kármán system and at $b/a = 0{\cdot}6$ the measured growth rate is larger. At $b/a = 0$ one vortex undergoes fission in the high-shear field produced by two nearest-neighbour opposite-signed vortex regions. Heuristic comparisons are made with the two-dimensional tunnel experiments of Taneda and others.

1. Introduction

In recent years there have been renewed efforts to understand the nonlinear dynamics of interacting vortex structures in high-Reynolds-number (high-R) two-dimensional jets and wakes. Carefully controlled experiments (Taneda 1959, 1965; Durgin & Carlson 1971) that minimize three-dimensional effects in low-noise wind tunnels have shown that asymmetric vortex structures have a finite lifetime, i.e. they become unstable. At variable distances downstream (many wavelengths of the fundamental vortex structure), the observed pattern abruptly loses its coherence and degenerates or 'breaks down into a less ordered pattern'. From this visually chaotic state evolves a secondary asymmetric vortex structure, more diffuse than the primary structure and of longer wavelength. This hierarchy

of two-dimensional vortex structures is sufficiently uncomplicated that a deterministic non-statistical approach should elucidate the basic mechanisms involved. As exemplified below, numerical simulations with a two-dimensional zero-viscosity model can provide some insight.

In flat-plate wake experiments, Sato & Kuriki (1961) also measured the properties of high-R wakes at moderate distances behind flat plates. Their high-quality hot-wire data were interpreted by Zabusky & Deem (1971) in a computational/experimental study as consistent with the motion of an asymmetric wake of elliptical nutating vortices. Zdravkovich (1968, 1969) and Durgin & Carlson (1971) also found elliptical and other distorted vortex structures to be a common occurrence in wakes behind cylinders. The elliptical shape of the vortices is a non-viscous effect due to the mutual interaction of nearby vortex regions.

To clarify the qualitative features of ideal high-R laminar flows downstream of *flat plates*, it is convenient to describe phenomena in contiguous spatial regions.

(i) At very short distances one finds nearly laminar flow with a Gaussian-type velocity profile. For $R > 10^4$ the inviscid Rayleigh equation provides eigenfunctions and unstable eigenvalues. R is based on the length of the plate. The Reynolds number based on the boundary-layer thickness is greater than 500.

(ii) At short distances, induced perturbations (via acoustically driven loudspeakers, vibrating ribbons, etc.) grow in accordance with linear stability theory. For $R > 10^4$ Sato & Kuriki (1961) and Zabusky & Deem (1971) showed that the Rayleigh equation provides unstable eigenvalues that agree with observations.

(iii) At moderate distances the fastest growing modes have the most energy and saturate when a regular asymmetric street of elliptical vortices forms. The finite-sized elliptical vortices undergo a slow pitching or nutating motion in the laboratory frame of reference. This phenomenon was also observed in the wake of cylinders and in two-dimensional jets by Beavers & Wilson (1970).

(iv) At large distances, the vortex structure may break down (collapse or undergo a transition) to another asymmetric street, where the longitudinal distance between nearby vortices in the same row can increase by a factor of 2–10 depending on the Reynolds number (Taneda 1959).

(v) At very large distances the breakdown and formation of the new vortex structure may be repeated several times. However, at very high R the turbulent or chaotic structure may persist.

In wakes beyond cylinders and other bluff bodies, regions (i) and (ii) are inseparable and pockets of vorticity can aggregate alternately on either side. At certain time intervals the upper and lower vortex concentrations are convected away to form an asymmetric street. For high Reynolds numbers, the rate of production of these vortex aggregations or the Strouhal number may be described by a vortex filament theory as shown by Gerrard (1967).

For high-R flows the above regions may not be clearly separated. The flow configuration at moderate to large distances (particularly at very high R) is very sensitive to the precise operating conditions and excitation mechanisms, that is, the predictability of the flow decreases at large distances or long times. The suppression of three-dimensional disturbances, the rigidity of the mounting,

the smoothness of the construction and excitation mechanisms, the quietness of the wind tunnel, and a finite viscosity all contribute to a more predictable result.

Computer simulation studies of the stability of wake-like configurations have been carried out for several years. A review of the efforts in this field has been given as an annotated bibliography by Harlow (1970). Calculations by Abernathy & Kronauer (1962) on the evolution of a laminar wake with a rectangular velocity profile arising from two rows of vortex filaments demonstrated the formation of the von Kármán vortex street. They also observed the capture or trapping of vortex filaments in regions of opposite-signed vorticity. This was also seen in calculations by Harlow & Fromm (1964), who studied the flow of a viscous heat-conducting fluid past a cylinder.

The linear stability theory for symmetric and asymmetric configurations of point vortices begun by von Kármán has been elaborated by Kochin (1939) and Kochin, Kiebel & Roze (1964). For two opposite-signed streets of point vortex filaments the symmetric configuration is unconditionally unstable. The asymmetric configuration on the other hand is only stable if the transverse-to-longitudinal separation ratio b/a is 0·281. However, as emphasized by Kochin *et al.* (1964, pp. 226–234), this is a necessary condition: "A first-order perturbation theory shows that the positions of vortices in a street with $b/a = 0{\cdot}281$ will separate by a finite amount." Rosenhead (1930) examined the linear stability of the $b/a = 0{\cdot}281$ asymmetric street for circular vortex regions of small but finite area. However, this calculation is *not* applicable to strictly two-dimensional *finite*-area vortex streets, as described below.

Most past analytical and computational work (Abernathy & Kronauer 1962) has concentrated on studying point vortex configurations, that is, vortex deformations are excluded from the dynamics. The reasons for excluding deformations of finite-area vortices can be summarized by quoting Bassett (1888, vol. 2, p. 42): "The mathematical difficulties of solving this problem when the initial distribution of the vortices and the initial forms of their cross-sections are given, are very great; and it seems impossible in the present state of analysis to do more than obtain approximate solutions in certain cases."

Our study generalizes and considers finite-area constant-density vortices (Rankine vortices; Lamb 1932, p. 29) confined by a contour

$$r^2(\theta) = R_0^2 + \sum_m \alpha_m e^{im\theta} + \text{c.c.},$$

where r is measured from the vortex centre. (The variable r^2 is used to simplify the verification of area conservation.) For $\alpha/R_0^2 \ll 1$ a translation with no distortion corresponds to an $m = 1$ disturbance and an $m = 2$ disturbance results in an elliptic shape. Generally, high-m disturbances can arise through close nonlinear interactions as shown by Christiansen & Roberts (1969) and by Christiansen (1973).

There has also been work on wake-like configurations. Using the VORTEX code, Christiansen (1970) studied the instability of a trapezoidal longitudinal velocity distribution with widely separated flanks and subject to random

perturbations. The final state was four staggered elliptically shaped vortices as found by Abernathy & Kronauer (1962, figures 10 and 11). Solving a finite-difference representation of the Navier–Stokes equation, Deem, Hardin & Zabusky (1971) initially perturbed a laminar Gaussian profile with a second harmonic plus a small random perturbation and observed the growth of four elliptically shaped vortices of unequal strength. There followed a period of quasi-stationary evolution of the vortex configuration and finally a rapid coalescence of pairs of like-signed vortex regions. Similar phenomena are described below in the simulations of a triangular velocity profile and the evolution of two pairs of opposite-signed asymmetrically placed vortex regions.

2. Two-dimensional motions in ideal fluids

The incompressible inviscid fluid (ideal fluid) can be described by the coupled continuity and Euler equations

$$\nabla . \mathbf{u} = 0, \tag{1}$$

$$\partial \mathbf{u}/\partial t + \mathbf{u} . \nabla \mathbf{u} = \rho^{-1} \nabla p. \tag{2}$$

For strictly two-dimensional motions the vorticity has one component in the z direction orthogonal to the plane of motion and one can introduce a stream function ψ:

$$\mathbf{u} = \nabla \times (\mathbf{e}_z \psi), \tag{3}$$

$$\zeta = \mathbf{e}_z . \nabla \times \mathbf{u} = -\nabla^2 \psi, \tag{4}$$

where

$$\nabla = \mathbf{e}_x \partial_x + \mathbf{e}_y \partial_y.$$

Substituting (3) and (4) into (2) yields the familiar Liouville equation (analogous to the one-dimensional Vlasov equation of plasma physics)

$$\zeta_t + \psi_y \zeta_x - \psi_x \zeta_y = 0, \tag{5}$$

which describes a Hamiltonian system with characteristic velocities

$$\dot{x} = \psi_y, \quad \dot{y} = -\psi_x. \tag{6}$$

Any state of the system is described by the vorticity distribution $\zeta(x, y)$ and can evolve into all other states subject to the constraints imposed by the conservation laws (integrals are taken over a finite region)

$$\mathbf{P} = \rho \iint \mathbf{u}\, dx\, dy \quad \text{(linear momentum)}, \tag{7}$$

$$\mathbf{L} = \rho \iint \mathbf{r} \times \mathbf{u}\, dx\, dy \quad \text{(angular momentum)}, \tag{8}$$

$$E = \tfrac{1}{2}\rho \iint |\mathbf{u}|^2\, dx\, dy = \tfrac{1}{2}\rho \iint \zeta \psi\, dx\, dy \quad \text{(kinetic energy)}. \tag{9}$$

$$\int A(\zeta)\, d\zeta = \text{constant} \quad \text{(vorticity areas)}, \tag{10}$$

where $A(\zeta)\, d\zeta$ is the area between two vorticity contours ζ and $\zeta + d\zeta$. Helmholtz's theorem tells us that these areas are convected with the fluid and hence it is convenient to study systems where the vorticity density ζ is constant and takes on the values $+\zeta_0$, 0 and $-\zeta_0$. The area conservation law is simply the conservation of area within the contours surrounding these regions.

The numerical experiments have been carried out with the particle/field (vortex filament–stream function or vorticity) VORTEX code (Christiansen 1970). This algorithm is based on the fact that the motion of vortex filaments is described by the ordinary differential equations (6). The stream function is

determined from the distribution of point vortices by numerically inverting the Poisson equation (4). The advantages and deficiences of this method were studied by Christiansen (1971) for the simple case of a single circular vortex of constant vorticity ζ_0 (Rankine vortex). The numerical experiments presented below have been carried out using 3200 positive or negative point vortices that were moved on a Cartesian mesh of dimensions 64×64. In general nine different types of boundary conditions were available. The appendix describes pertinent details of the code's operation.

Errors are inevitable in solutions produced by finite-difference methods. In the VORTEX code no attempt is made to enforce conservation or 'semi-conservation' (continuous temporal variables) of mass (local incompressibility of the flow), momentum, energy, enstrophy (Leith 1968) or area. These quantities are monitored to allow one to assess the quality of the run (see appendix). Although the velocity field calculated at the mesh points is solenoidal, the interpolations used to extract the velocity of a vortex filament introduce a local violation of incompressibility which is manifest in the figures below as a fine wavelike structure, particularly on the surface of the vortex region. One easily resolves this structure on the large-area vortices, e.g. figure 5 ($t = 8{\cdot}75$), figure 6 ($t = 7{\cdot}5$) and figure 10 ($t = 7{\cdot}0$). Note that the fine structure becomes sharper and penetrates deeper into the vortex regions at later times; see figure 4 ($t = 8{\cdot}75$). Also long 'arms' of vorticity are dispersed, indicating that small-scale phenomena are not adequately represented. These short-wavelength truncation errors do not cause instability and apparently do not contribute greatly to the large-scale motions for the duration of our runs.

3. Epitome of numerical experiments

The numerical experiments summarized in this section and outlined in table 1 are all related to our abstractions of high-R wakes behind flat plates or bluff bodies. These are initial-value problems and in discussing laboratory experiments we assume that the time elapsed in a calculation corresponds to distance downstream. Zabusky & Deem (1971) validated this assumption by comparing numerical solutions of the Navier–Stokes equation with the flat-plate wake experiments of Sato & Kuriki. The calculations start from uniform vorticity distributions located in a box with periodic boundary conditions in x and either fixed or periodic boundary conditions in y. Equations (4) and (5) are normalized such that a vorticity density $\zeta_0 = N/A$ (N = number of point vortices confined to the area A) will produce a rotational period of $T_0 = 4\pi/\zeta_0$ units of time. The time step in an integration initially satisfies the Courant–Friedrichs–Lewy condition by a wide margin and is taken as

$$\Delta t = C\,\Delta x/\langle|\mathbf{v}|\rangle = (4\langle|\mathbf{v}|\rangle)^{-1}, \tag{11}$$

where

$$\langle|\mathbf{v}|\rangle = \frac{1}{N}\sum_{j=1}^{N}|\mathbf{v}_j|. \tag{12}$$

In §5 we discuss the laminar triangular longitudinal velocity profile with random perturbations (experiment I) and show that the linearly unstable profile

Expt.	b/a	Eccentricity of vortices	π^{-1} (area of typical vortex)	y boundaries	Elapsed time, T_E	Number of time steps	ζ_0	T_E/T_0
I	Laminar wake		–	F	10·5	1344	6·25	
II	0·281	0·0	9	F	9·0	576	27·0	19·4
III	0·281	0·0	35	P	9·0	576	7·0	5·0
IV	0·281	0·85	26	F	3·0	192	9·4	2·24
V	0·281	0·85	26	F	3·0	192	9·4	2·24
VI	0·6	0·7	35	F	24·0	768	7·0	13·3
VII	0·6	0·7	35	P	6·0	192	7·0	3·3
VIII	0·6	0·0	35	P	6·0	192	7·0	3·3
IX	0·6	0·0	9	P	9·0	1152	27·0	19·4
X	0·0	0·0	35	P	17·0	576	7·0	9·45

TABLE 1. Experiments presented in this paper. In column 5, F and P mean fixed or periodic y boundaries. In column 9, $T_0 = 4\pi/\zeta_0$ is the rotation period of the vortex.

transforms into an asymmetric (staggered) array of unequal-strength vortex regions which coalesce or fuse.

In § 6 we begin the study of the stability of four finite-area vortex regions, with periodic boundary conditions in the longitudinal (x) direction. The circulation of each vortex is $\Gamma_0 = \pi R_0^2 \zeta_0 = 766$. The parameters of the study are the following.

(i) The area of the vortex regions.

(ii) The initial shape of the regions.

(iii) The transverse boundary conditions (fixed or periodic).

(iv) The nature of the perturbation to one or more vortex regions (lateral or longitudinal displacement of the centroid of a vortex region, shape or size change, etc.).

(v) The transverse-to-longitudinal separation ratio b/a of the vortex centres.

Section 6 studies the case $b/a = 0{\cdot}281$ (experiments II–V), known to be least stable for point vortices. For runs of duration 19 circulation periods, we find stability.

In § 7 we treat the case $b/a = 0{\cdot}6$, known to be unstable for point vortices, and we find instability followed by fusion of like-signed vortices. See experiments VI–IX.

In § 8 the standing-wave case $b/a = 0$ is treated and we find instability and a peculiar strong dynamical interaction that finally leads to a rapid fission of one vortex followed by fusion of vortex regions on a longer time scale. See experiment X.

The results are visualized by displaying the location of vortex filaments (particles) at separated times. Dark grey areas represent regions of negative vorticity (clockwise rotation) and light grey areas represent regions of positive vorticity (counterclockwise rotation); see figures 2, 4–8 and 10. A computer-generated film has been made that vividly demonstrates many of the phenomena. K. V. Roberts showed and discussed this film at the European Conference on Computational Physics (Geneva, April 1972) as part of his talk on a review of numerical methods in fluid dynamics (Roberts & Christiansen 1972).

4. Comments on previous analytical work

The original calculation by von Kármán for an asymmetric point vortex system has been repeated by Lamb (1932, § 15*b*, p. 228) and somewhat generalized by Kochin *et al.* (1964, § 5.21). If neighbouring vortex filaments on the same line (separated by a) are given the same displacement $x_m = \alpha e^{im\phi}$, $y_m = \beta e^{im\phi}$, the solution of the linearized perturbation equations yields the dispersion relation

$$\lambda = (\Gamma_0/2\pi a^2)\,[\pm iD \pm (A^2 - C^2)^{\frac{1}{2}}], \tag{13}$$

where

$$A = \tfrac{1}{2}\phi(2\pi - \phi) - \pi^2/\cosh^2(\pi b/a), \tag{14}$$

$$B = iD = i\left\{\frac{\pi\phi \sinh(\pi - \phi)\, b/a}{\cosh(\pi b/a)} + \frac{\pi^2 \sinh \phi b/a}{\cosh^2(\pi b/a)}\right\}, \tag{15}$$

$$C = \frac{\pi^2 \cosh(\phi b/a)}{\cosh^2(\pi b/a)} - \frac{\pi\phi \cosh(\pi - \phi)\, b/a}{\cosh(\pi b/a)}. \tag{16}$$

The condition $\phi = \pi$ is most unstable as it makes $C = 0$ and

$$A = \tfrac{1}{2}\pi^2[1 - 2\cosh^{-2}(\pi b/a)], \tag{17}$$

$$B = iD = i\pi^2[\sinh(\pi b/a)\cosh^{-2}(\pi b/a)]. \tag{18}$$

The condition $A = 0$ is necessary for stability and this yields the well-known condition

$$\cosh(\pi b/a) = 1 \quad \text{or} \quad b/a = 0{\cdot}281. \tag{19}$$

The oscillation frequency is

$$\operatorname{Im}\lambda = \pm \tfrac{1}{4}\pi\Gamma_0/a^2 = \pm 0{\cdot}5895, \tag{20}$$

where the numerical value corresponds to our case, $a = 32$ and $\Gamma_0 = \pi R_0^2 \zeta_0 = 766$ (the number of filaments in each vortex region). The growth rates at two values of b/a are

$$\lambda = 0{\cdot}481 \quad \text{for} \quad b/a = 0{\cdot}6, \tag{21}$$

$$\lambda = \tfrac{1}{4}\pi\Gamma_0/a^2 = 0{\cdot}590 \quad \text{for} \quad b/a = 0. \tag{22}$$

Three additional analytical calculations are relevant to the results below. Kochin *et al.* (1964, pp. 226–234) applied a higher order perturbation calculation to the asymmetric point vortex street with $b/a = 0{\cdot}281$. They have shown that the street is always *unstable*, i.e. arbitrary small displacements will cause vortices to "... separate by a finite amount". This is not surprising as the Kármán street is unstable for $b/a \gtrless 0{\cdot}281$. If odd vortices on the upper street are displaced upwards by ϵ a configuration results which is identical to that obtained by increasing the separation to $0{\cdot}281 + \frac{1}{2}\epsilon$ and then displacing positive vortices upwards by $\frac{1}{2}\epsilon$ and negative vortices downwards by $\frac{1}{2}\epsilon$. Since the latter system is linearly unstable, it would be reasonable to assume that the former system is unstable to finite-amplitude disturbances.

Rosenhead has extended the von Kármán linear analysis by examining the effects of transverse free-slip boundaries (1929) and the effects of three-dimensional/small-area regions (1930). In the first study Rosenhead assumed point vortices such that, if fixed y boundaries are introduced at a distance $\pm \frac{1}{2}h$ from the centre of the street, the b/a ratio for 'stability' decreases from 0·281 to 0·256 as a/h increases from 0 to 0·815. As a/h is increased further, the b/a *line* becomes

a *region* or area of stability. Rosenhead gives a formula for the modified stability line as

$$b/a = 0{\cdot}281 - 0{\cdot}090(a/h)^6 = 0{\cdot}280,$$

where we have used our ratio $a/h = 0{\cdot}5$. (See Rosenhead (1929, equation (5), p. 321). Note that Rosenhead used $2b$ for the *longitudinal* distance between vortices, $2a$ for the *transverse* distance between vortices and $2c$ for the distance between the fixed walls.) In comparison with finite area the transverse boundaries play a negligible role.

In the second study Rosenhead (1930) considered the behaviour of small circular vortices of radius $\epsilon = R$, where $\epsilon/a \ll 1$. He assumed that vortices have azimuthal ($m = 1$) self-interactions ('self-induction') resulting only from z-direction perturbations of wavelength $L_z = 2\pi l^{-1}$. (See Rosenhead 1930, pp. 595, 599.) Rosenhead defined a parameter

$$\eta_R = -\tfrac{1}{2}a^2 l^2 \log(\epsilon l), \quad \epsilon l < 1,$$

where ϵl is assumed small and $\eta_R > 0$. The larger η_R, the stronger is the self-induction.

Physically, one must consider at least four different length scales:

$$A_{vm} < \epsilon < a < L_z,$$

where A_{vm} is the amplitude of the perturbation of the mth azimuthal harmonic on the vortex surface and the remaining quantities have been previously defined. If L_z and ϵ are of comparable size and $al \gg 1$, then η_R will be larger than unity and three-dimensional effects will be important. However, if L_z is increased ($al \ll 1$) and ϵ/a is kept fixed, then the parameter which describes self-induction will be dependent on A_{vm}, ϵ, a and b and only weakly dependent on al. For two vortices of the same sign an important parameter is

$$\eta = 2R/a \equiv 2\epsilon/a$$

(Christiansen 1973) as described in § 8. Thus, Rosenhead's (1930, p. 599) claim that for $\eta_R \to 0$ the stability analysis reduces to von Kármán's is incomplete for it implies the limit he used, namely $A_{vm} = 0$ ($m \neq 1$), $\epsilon l < 1$, $al > 1$ (such that $\epsilon/a \ll 1$); whereas all the work reported below assumes two-dimensionality, that is $l \equiv 0$ and $\epsilon l = 0$, $al = 0$ and $\epsilon/a < 1$ but comparable with $\frac{1}{4}$ in some cases.

5. Laminar wake with a triangular velocity profile

To simulate a laminar triangular velocity profile with a random perturbation, we distribute uniformly 1600 positive (light) and 1600 negative (dark) point vortex filaments over an area 8×64 as shown in figure 1 (a). This results in two strips of vorticity density $\zeta_0 = \pm 6{\cdot}25$. The laminar state is perturbed by a random and incompressible velocity field producing an average displacement of 10^{-2} of each filament.

Figure 1 (b) shows the longitudinal velocity profile obtained by integrating the resultant ζ and choosing the constant of integration to result in zero x momentum.

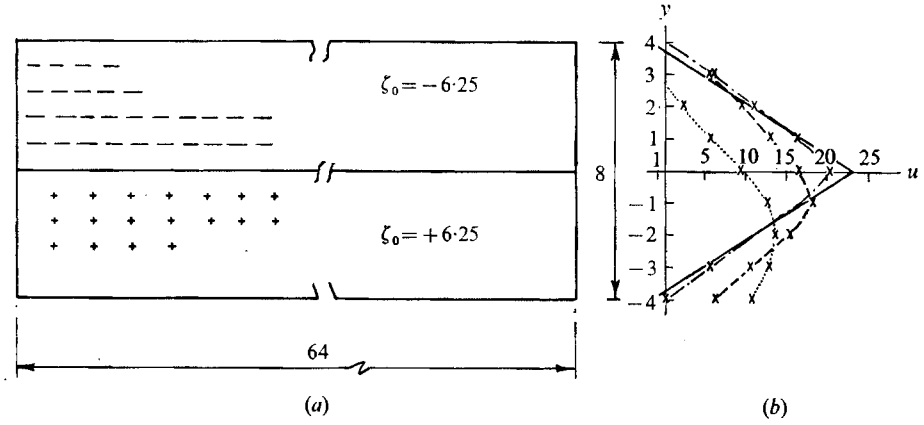

FIGURE 1. Experiment I. (*a*) Initial distribution of vorticity (x-periodic box). (*b*) Initial velocity profiles at $x = 32$. ——, theoretical; – – –, $t = 0{\cdot}125$; — — —, $t = 4{\cdot}0$; ·····, $t = 6{\cdot}0$.

The initial departure from the triangular profile is caused by the random perturbation as well as by the area-weighting method mentioned in the appendix.

The evolution of the perturbed triangular profile is shown in figure 2. We shall not discuss the linear phase of evolution as it has been well treated elsewhere (for example, Zabusky & Deem 1971). After approximately $t = 4{\cdot}2$ the perturbation has grown and saturated because of nonlinear effects. At $t = 4{\cdot}75$ we see that four negative and four positive elongated vortex regions of varying area have formed into an asymmetric pattern. Note that at this stage small areas of positive or negative vorticity become 'trapped' within or behind the larger vortex of opposite polarity. Between $t = 5{\cdot}0$ and $6{\cdot}75$ two negative vortex regions (2 and 3) fuse into an elongated structure. At $t = 6{\cdot}75$ we see positive vortex regions (5 and 6) begin to fuse. At $t = 7{\cdot}75$ vortex region 1 is beginning to fuse with regions 2–3, but the process is inhibited by regions 5–6. Note that at $t = 7{\cdot}75$ the approximate transverse-to-longitudinal separation ratio is $\bar{b}/\bar{a} = 0{\cdot}42$, that is, the wake width has increased by a factor of three owing to the fusion, elongation, rotation and jetting of vortex 'streams' or 'arms', that is, by *convective* processes. After $t = 8{\cdot}0$ we have an irregular structure of three negative and three positive vortices per period with some mixing of positive and negative vortex filaments between the larger vortex regions. The situation corresponds roughly to an array of vortices staggered with respect to each other and moving in a weakly turbulent flow caused by 'dispersion' of vortex filaments. This situation still prevails at $t = 10{\cdot}5$ (not shown in figure 2) with more filaments dispersed away from the main regions. Numerical finite-difference effects contribute to this dispersion and mixing of filaments and can be observed at $t = 7{\cdot}0$. However, for a short time the intermixing of the small-scale chaotic motion does not affect the mean behaviour of the large-scale vortex structures.

In figure 2 at $t = 4{\cdot}75$ we see that negative vortex 4 is elongated and its major axis rotates clockwise at a non-uniform rate whose average period is 4·7 (measured over the range $4{\cdot}75 < t < 10{\cdot}25$). A non-interacting ellipse (Kirchoff vortex; Lamb 1932, p. 230) has a period $T_2 = (4\pi/\zeta_0)(\mu+1)$, where $\mu = (2-e^2)/2(1-e^2)^{\frac{1}{2}}$,

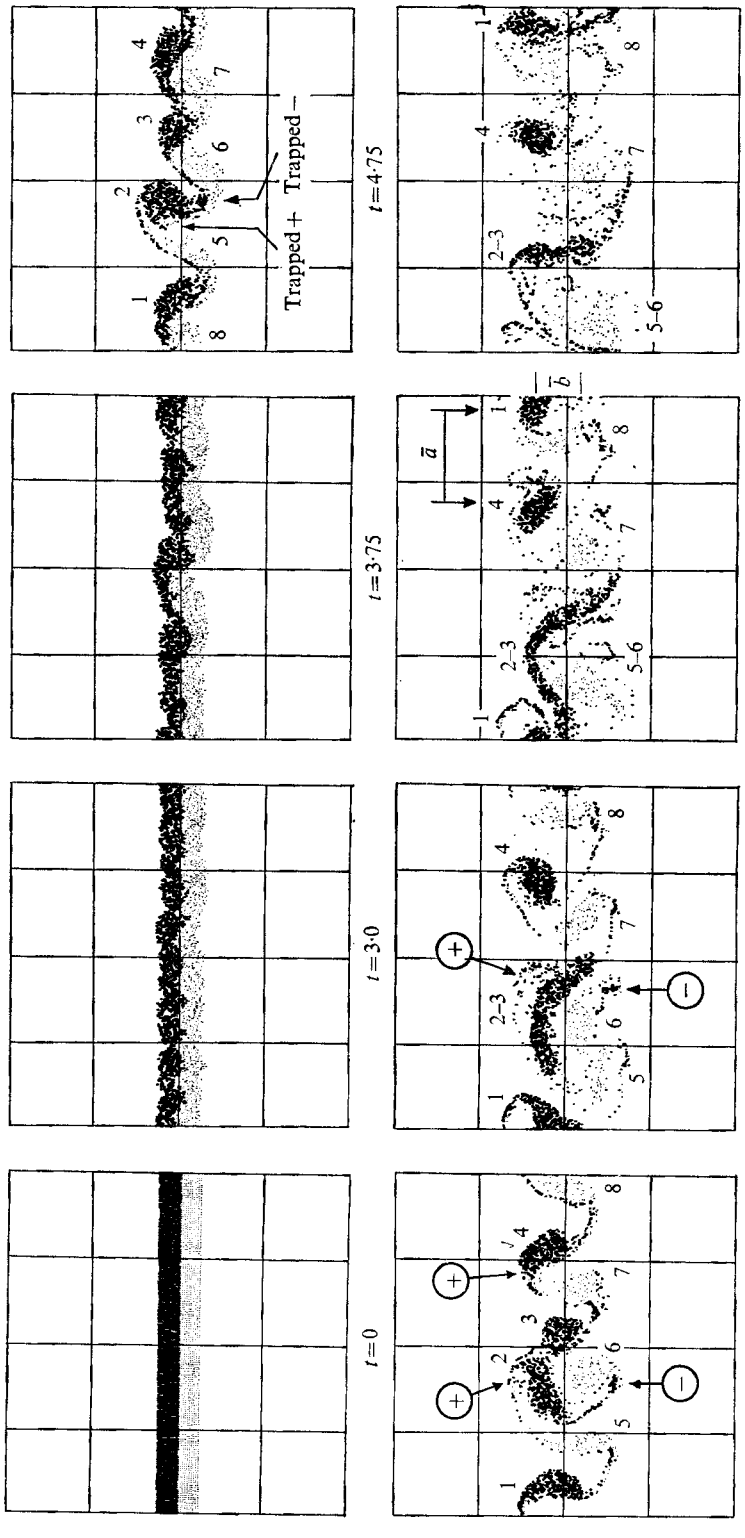

FIGURE 2. Experiment I. Instability of a laminar wake subject to a small random perturbation. Fixed y boundaries.

ϵ being the eccentricity of the ellipse. A rough estimate of vortex 4 gives $\epsilon^2 = 0{\cdot}75$, so that $T_2 = 4{\cdot}52$, close to that of the deformed strongly interacting elongated vortex region. Note that all vortex regions are drifting slowly to the left, whereas the distant irrotational fluid is streaming uniformly to the right.

In figure 2 we observe that small trapped regions are convected around at the rotational frequency of the opposite-signed host vortex. This phenomenon was also observed and noted by Zabusky & Deem (1971) and they designated these small regions as 'secondary' vortices (see their figure 8, p. 368). Owing to vortex rotation (in an appropriate frame) or 'nutation' in the laboratory frame of reference, tracer particles, smoke or single vortex filaments will be transported to the opposite side of the vortex street. This phenomenon has been observed by Zdravkovich (1969, § 3 and figure 3) and can also be seen in figure 11 of Abernathy & Kronauer (1962). Thus we have an enhanced transport of material across a flow due to convection by vortex states formed as a result of a linear instability of the system.

A comparison between this calculation and that of Abernathy & Kronauer (1962), which starts off from a rectangular velocity profile, is difficult. Some measure of agreement can be established with the calculation shown in their figure 11. The spacing ratio $\bar{b}/\bar{a}$ far downstream in the wake is found to be approximately 0·5 as opposed to our value of 0·42. It is, however, difficult to assess their value of $\bar{b}/\bar{a}$ (as they mention), since the centres of the vortices formed are not well defined by the very small number of filaments (typically 10 as opposed to 400 in our calculation).

To summarize, in the early stages the linear instability driven by a particular random perturbation yields eight large vortices staggered with respect to each other. At $t = 5{\cdot}75$ all vortices are elongated and nearly elliptical in shape but with different phases. The magnitude of the phases as well as the transverse separation between the vortices is a result of the initial conditions. This structure is unstable and like vortices are attracted and fuse in an attempt to find a more stable configuration. This transition from one vortex state to a more enduring state provides a heuristic explanation for the observations of Taneda (1959, § 3, p. 847). At intermediate ($100 < R < 150$) and high ($R > 150$) Reynolds numbers the vortex streets in the wakes of cylinders (and flat plates) break down and reform such that the ratio of the effective wavelength of the secondary street to that of the primary street is two for intermediate R and "... of order 10" (according to Taneda) for high R. The intermediate-R result could be explained as merely the fusion of nearest-neighbour like-signed vortex regions as observed above or as more clearly observed later in this section. That is, viscous dissipation plays a small role in comparison with the convective dynamical rearrangement of vortex filaments. Taneda observes this rearrangement or breakdown to occur again further downstream, a phenomenon consistent with our calculations. Taneda's high-R result is phenomenologically different for "... after the primary Kármán vortex street breaks down the wake becomes turbulent, ...[a result already noted by Roshko in 1953].... The turbulent wake continues to exist for a considerable distance, then there appears again a new Kármán vortex street." In the laboratory, the wake may develop small three-dimensional

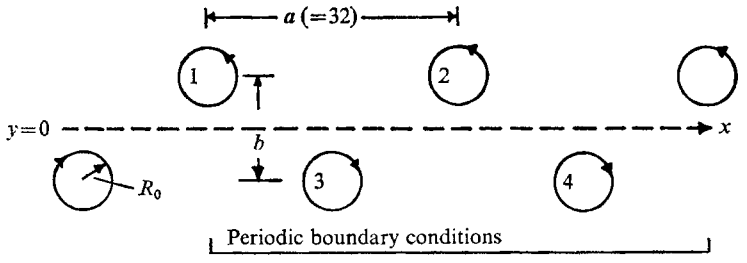

FIGURE 3. Arrangement of vortices.

destabilizing fluctuations that enhance the fusion of larger vortex regions over a moderate distance. The enhancement process will cease when the three-dimensional fluctuations undergo viscous decay and we are left with a new two-dimensional quasi-equilibrium state.

6. Configurations of least instability

We now study the stability and dynamics of two pairs of Rankine vortices of radius R_0 and density $\pm\zeta_0$. As shown in figure 3, they are placed in a staggered fashion in a box with periodic boundary conditions in x, simulating states encountered in laboratory and computational experiments as described above.

Our realistic model considers finite-sized vortices. If initially circular, their radius R_0 is less than

$$R_M = \tfrac{1}{4}a(1+4b^2/a^2)^{\frac{1}{2}} = 9{\cdot}17 \quad \text{for} \quad a = 32, \quad b/a = 0{\cdot}281,$$

if they are non-overlapping. The radius function of a vortex during the subsequent motion can be written as

$$r^2 = R_0^2 + \Sigma\alpha_m e^{im\theta}, \tag{23}$$

where r is measured from the initial centre of the vortex

$$r_c = \frac{1}{2\pi}\int_0^{2\pi} \tilde{r}(\theta)\,d\theta.$$

The deformation of a vortex by a surface mode α_m decreases the energy of the vortex; hence the mode can be referred to as a *negative-energy* mode (Christiansen 1973). For incompressible fluids there is no $m = 0$ mode and expression (23) conserves area $\left(= \frac{1}{2}\int_0^{2\pi} r^2(\theta)\,d\theta = \pi R_0^2\right)$. It is natural to ask: how does the finite area of vortex regions affect the von Kármán stability conditions? The instability that leads to a rearrangement of the street results from a growth of the $m = 1$ mode for one or more vortices [see equation (23)].

We have performed four different numerical experiments all using $b/a = 0{\cdot}281$ in order to examine the stability properties of the arrangement sketched in figure 3. Experiments II and III have initially four circular vortices of radius 3·0 and radius $(35)^{\frac{1}{2}}$, respectively. In experiment II we introduce fixed y boundaries, whilst III employs a double periodic geometry. The perturbation is in both cases

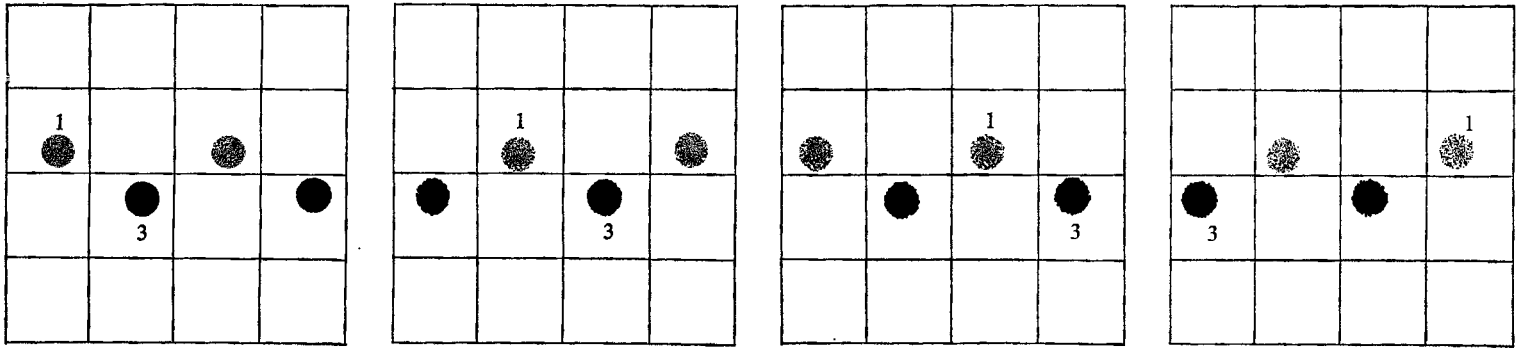

$t=0$ $t=2{\cdot}75$ $t=5{\cdot}75$ $t=8{\cdot}75$

FIGURE 4. Experiment II. Small vortices. $b/a = 0{\cdot}281$. Fixed y boundaries.

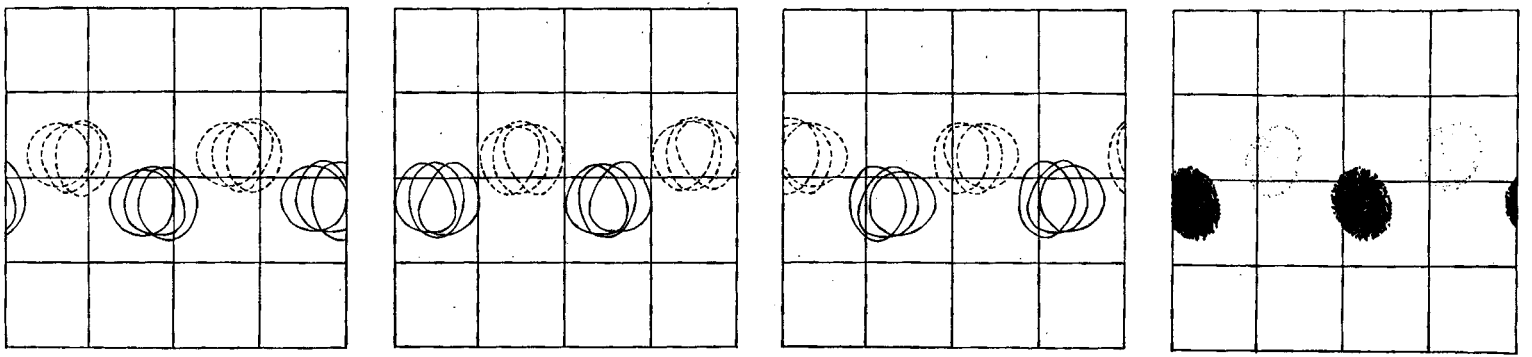

$t=0,\ 0{\cdot}5,\ 1{\cdot}0$ $t=2{\cdot}5,\ 3{\cdot}0,\ 3{\cdot}5$ $t=5{\cdot}0,\ 5{\cdot}5,\ 6{\cdot}0$ $t=8{\cdot}75$

FIGURE 5. Experiment III. Large vortices. $b/a = 0{\cdot}281$. Periodic y boundaries. The first three frames show only the vortex boundaries. The left most contour refers to the smallest time indicated.

a displacement of 1·0 in the y direction of vortex 4, that is, an $m = 1$ disturbance. Both experiments last for a time interval of 9·0, corresponding to 576 discrete time steps (see table 1). In experiments IV and V we introduce very strong asymmetric perturbations: in experiment IV the major axes of positive vortices are inclined at 0·2 rad, whereas the major axes of negative vortices 3 and 4 are inclined at $-0{\cdot}2$ and 0 rad. In experiment V the major axis of vortex 1 reduced from 7 to 4 so that the resulting density becomes $\frac{7}{4}$ times that of the other three vortices. In both experiments vortex 4 is given a *longitudinal* displacement (also an $m = 1$ disturbance) of $-6{\cdot}0$. Experiments IV and V last only for a time interval of 3·0.

From figures 4 and 5, displaying the time evolution of experiments II and III, it can be seen that both flow fields are apparently stable with respect to a small transverse perturbation. For all four vortices in *both* experiments the amplitude of the perturbation (say the position of the lowest point on the boundary) is found to be 1·0 (the same as the initial amplitude) and the period is 11·0. This is in good agreement with the result given in (20): $T = 2\pi/\mathrm{Im}\,(\lambda) = 10{\cdot}7$.

In both experiments the vortices rotate, deform and drift to the right with velocities nearly independent of their areas. Surface modes $m = 2$, 3 and higher develop from the mutual interactions of vortices. This is illustrated in figure 5, where the first three frames each show only the boundaries of the vortex regions at three close times (the leftmost contour is for the smallest of the times indicated). The amplitudes of the surface modes oscillate with time, such that after one period of rotation T_0 the circular form is reached again. The period T_0 is 1·9. For a non-interacting vortex in an infinite medium the period is 1·8 (table 1). The difference is due to nonlinear effects as well as coupling between modes of different m (see also § 8).

The fine-scale structure and surface corrugations that develop (as exhibited at $t = 8{\cdot}75$) are due to numerical area-weighting effects and do not disturb the large-scale dynamics.

Experiments IV and V (figures not shown), with different initial conditions and *strong* perturbations, show similar effects, namely rotation, deformation and translation. In these short runs we observe an oscillation period of 8·0 (instead of 11·0) and no sign of a growing perturbation. This may be a finite-amplitude effect, however, the run duration is too small to make a definitive statement. The difference in periods could also be a measurement error since we have less than $\frac{1}{4}$ period of information.

The effect of the finite-difference algorithm on the small growth rates of a marginally stable system must be assessed. The variety of results presented here and the fact that parts of the vortex regions obviously extend into regions that are unstable for the point vortex system lead us to conclude that the observed stability is a property of the continuum, namely equation (2). The existence of *negative-energy* modes resulting from area-conserving surface deformations (Christiansen 1973) contributes to this stability if the initial finite-amplitude disturbance is not too large. We conclude that high-R finite-area vortex streets have a small domain of stability around $b/a = 0{\cdot}281$.

Experiment	Figure	Area	Boundary condition	Perturbation	Measured growth rate, λ_m	Approximate fusion time
VI	6	Large	Fixed	Large	0·62	5·5
VII	7	Large	Periodic	Small	—	5·8
VIII	7	Large	Periodic	Small	0·67	5·8
IX	8	Small	Periodic	Small	0·67	6·9

TABLE 2

7. Unstable configurations

We have performed four experiments with $b/a = 0{\cdot}6$ as summarized in table 2.

In figure 6 we display the time evolution of experiment VI, whilst figure 7 shows both experiments VII and VIII. Experiment IX, employing small vortices, is shown in figure 8.

Experiments VI, VII and VIII, for the large-area vortices, all show fusion of positive regions at about $t = 5{\cdot}5$ (fixed boundary condition) and $t = 5{\cdot}75$ (periodic boundary condition). Experiment IX, for the small-area vortices, shows fusion at about $t = 6{\cdot}87$ (15 vortex rotations). The initial positive vertical perturbation of the centre of vortex 4 is rapidly communicated to vortex 2, which, while being ejected from the flow, attracts vortex 1. In experiment VI, although vortices 3 and 4 are close together at $t = 6{\cdot}0$, the dynamics do not allow fusion until $t = 19{\cdot}5$.

In figure 9 we show the Δy_c of vortex 1 (moving downwards) for experiments VI, VIII and IX. Δy_c is the difference between the ordinates of the centres of the vortices,

$$\Delta y_c = y_c(t) - y_c(0),$$

as measured from enlarged figures similar to those given in this paper and has an accuracy of $\pm 0{\cdot}3$ units. The motion of the lower vortices 3 and 4 is initially oscillatory. The measured growth rate given in table 2 shows a larger value for the larger area vortex and both values are about 30% larger than the 0·481 for the point vortex system. This increase is undoubtedly due to the facts that the vortex extends into 'more unstable' regions, that is, where the 'effective' growth rate experienced by a point vortex is larger than that experienced by a point vortex at the centre of the finite-area region; and finite-amplitude effects are important early in the dynamics. (Note that, at $t = 2$, $\Delta y_c = 2{\cdot}5$ units.)

At later times when the dynamics are nonlinear and there are large distortions to the vortex surface ($m = 2, 3, \ldots$), the rate of approach of like-signed large vortices is enhanced, leading to a smaller fusion time. We find no significant change in the growth rate when the area is changed by a factor of $\frac{3.5}{9}$.

Beyond fusion, in the interval $t = 7$–19 (see figure 6) the centroid of the fusion vortex is nearly stationary at the upper right and the two remaining vortices undergo precession. When they approach after $t = 7{\cdot}5$, the vortex nearest to the fusion vortex is perturbed by the latter, i.e. a large $m = 2$ mode develops.

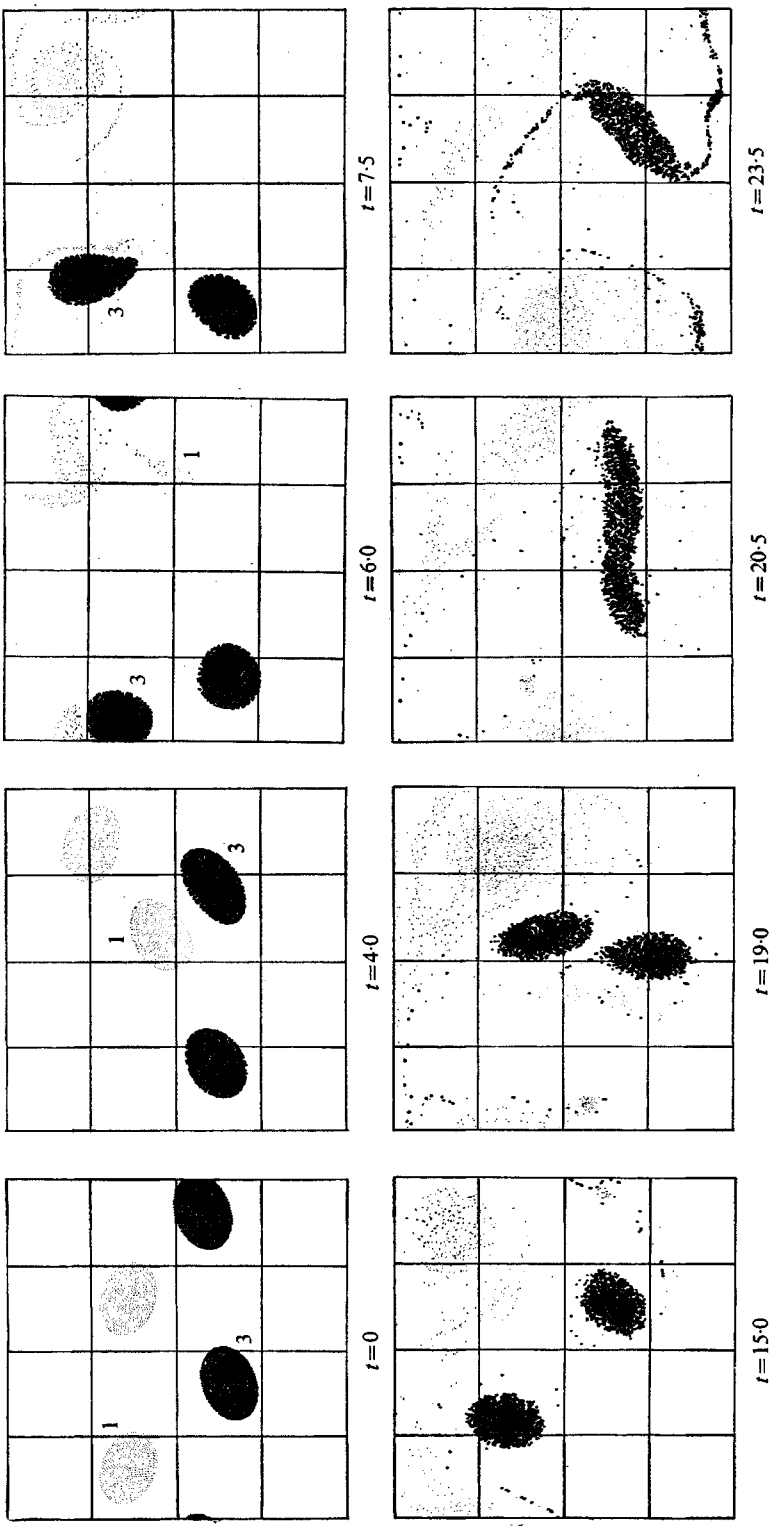

FIGURE 6. Experiment VI. Large vortices. $b/a = 0{\cdot}6$. Fixed y boundaries.

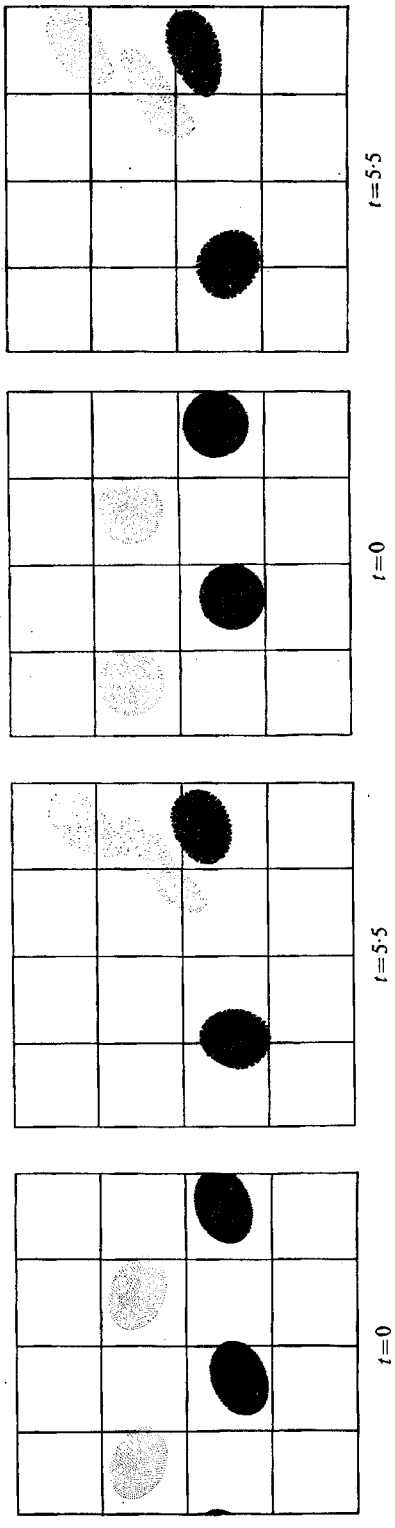

FIGURE 7. Two initially different unstable configurations. $b/a = 0{\cdot}6$. Periodic y boundaries.

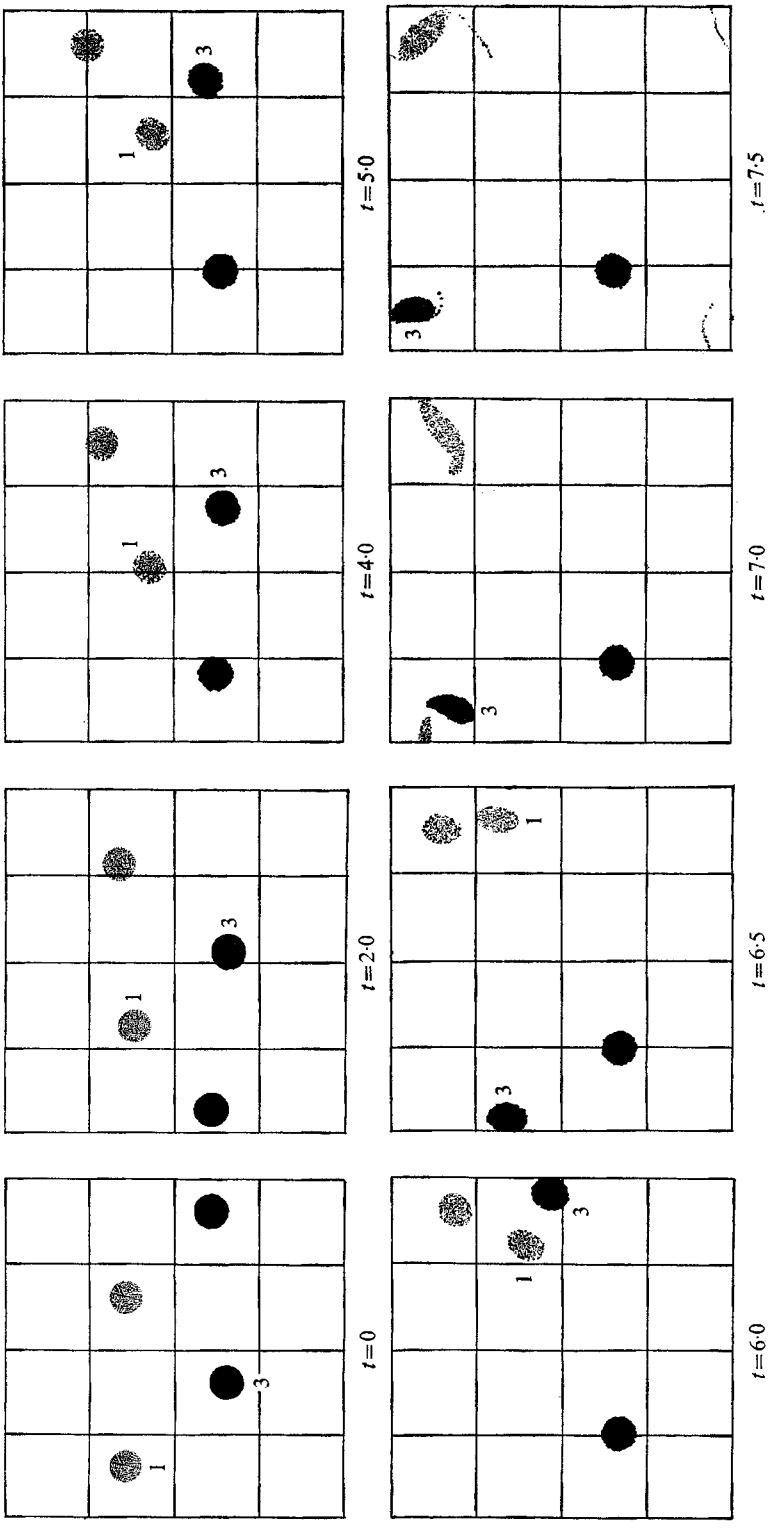

FIGURE 8. Experiment IX. Small vortices. $b/a = 0{\cdot}6$. Periodic y boundaries.

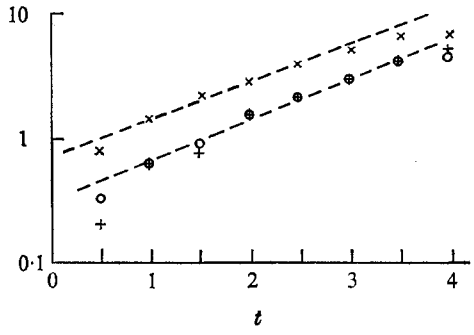

FIGURE 9. Growth of vortex centre deviations Δy_c and measured growth rates for systems with $b/a = 0{\cdot}6$. ×, experiment VI; +, experiment VIII; ○, experiment IX.

At $t = 18{\cdot}5$ the two negative vortices have completed a full precession around their mutual centre and have also moved $\frac{1}{3}$ of the period in the $+x$ direction. The upper vortex and the fusion vortex now form a binary system which travels downward. The lower vortex cannot move further downward (fixed boundary condition), hence the two negative vortices fuse. The elongated shape of the resulting vortex at $t = 20{\cdot}5$ is a result of the lower y boundary being fixed, since a circular or slightly elliptic shape would give rise to a net motion towards the lower boundary. At $t = 23{\cdot}5$ we note that the elongated vortex has contracted and thrown off spiral arms. The final result is then a 'secondary' vortex street, with larger regions of positive and negative vorticity in asymmetric or staggered positions.

The dispersion and mixing of small-scale positive and negative vortex filaments between the larger vortex regions are strongly affected by numerical truncation errors, but play an insignificant role. This is analogous to real systems with finite but high R where small scales are dissipated. Two-dimensional fluid dynamic systems are known to seek states with larger scales (energy flowing to longer modes). This represents a new kind of condensation phenomenon.

8. Collinear asymmetric street of strongly interacting vortices

The collinear ($b/a = 0$) asymmetric vortex street (see figure 10) is initially a standing wave with zero velocity:

$$V_0 = (\Gamma_0/2a)\tan h(\pi b/a) = 0.$$

Koopman (1967, p. 508) has shown that configurations with a small value of b/a can be generated in the laboratory by oscillating the cylinder transverse to the direction of flow. (In essence pockets of vorticity are detached from the cylinder at times that correspond to the transverse motion of the pocket across the axis of the flow.) Recently experiments have been made by Griffin & Votaw (1972) on the generation of vortex streets with small b/a values. Their figure 8 shows an almost collinear vortex street, but with a small value of the interaction parameter $\eta = 2R/a$ (see § 4 above). The evolution of this vortex street agrees with previous observations, and the general character of the breakdown resembles those of the configurations studied in § 7.

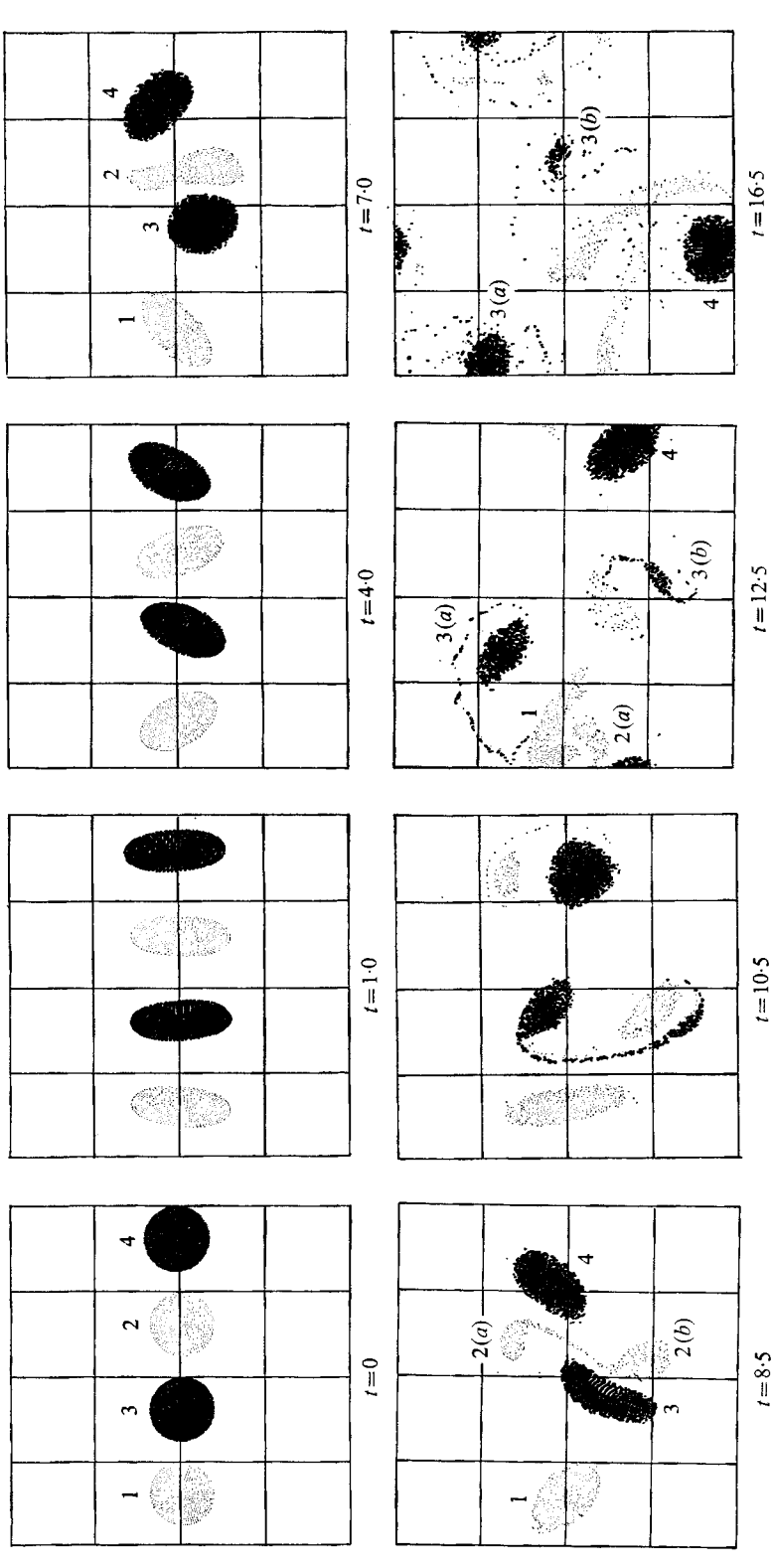

FIGURE 10. Experiment X. Large vortices. $b/a = 0$. Periodic y boundaries.

The collinear vortex street pictured in figure 10 has a high initial value of η thereby enhancing the self-induction effects mentioned in §4. The results obtained in our experiment X show linear instability regions followed by a strikingly new phenomenon: the fission of one vortex.

A transverse perturbation is given to vortex 4 (the fourth on the line) and it grows during $0 < t < 6{\cdot}0$, while the centre of vortex 3 is slightly displaced downwards. The measured initial growth rate is

$$\lambda_m = 0{\cdot}41,$$

smaller than the point vortex value of 0·59.

Qualitatively, one may explain this reduction by noting that the outer areas of the collinear vortices are in spatial regions where the growth rate of a point vortex is *smaller*. That is, a first approximation to the growth rate of a finite-area system may be obtained by weighting the vorticity distribution with the growth rate due to that vorticity treated as a point vortex system.

The strong perturbations (mainly $m = 2$) that develop because of the close interaction between the vortices get increasingly out of phase as the applied disturbance grows. At $t = 7{\cdot}0$ the phase difference between the $m = 2$ mode on vortex 2 and those on vortices 3 and 4 is a maximum. This causes a stretching followed by fission of vortex 2 in the strongly sheared velocity field. The upper fission product is left nearly free while the lower fission product is trapped below vortex 3. At $t = 12{\cdot}5$ the upper fission product fuses with vortex 1 and much later at $t = 16{\cdot}5$ the lower fission product fuses with vortex 1. At this time we still have a fission product from vortex 3 in the centre of the frame.

The fission of large-area vortex regions is the result of strong interactions with nearby vortex regions (large η). It is strictly a two-dimensional phenomenon, i.e. it is subject to the correct phase mixing of perturbations which typically remain two-dimensional over a time period of two vortex rotations. For smaller values of η only the predicted $m = 1$ instability occurs, leading to a breakdown pattern as observed by Griffin & Votaw (1972) and also in our experiments VI–IX. Thus the stability properties of a collinear vortex street *strongly* depend on η; indeed a truly nonlinear situation.

9. Discussion and conclusion

In this paper we have shown that the measured growth rates of finite-area vortex streets differ from those of corresponding point vortex systems (von Kármán systems). For small and moderate areas (small η) the difference is weakly dependent upon area and shape, but strongly dependent upon $(b/a)_c$ as illustrated in figure 11. In this figure we conjecture that there exists a region (α_1, α_2) on the b/a axis,

$$\alpha_1 < 0{\cdot}281 < \alpha_2,$$

where the growth rate is negative, that is, the presence of negative-energy modes on the surface of finite-area vortex systems is stabilizing.

Furthermore, because the vorticity is distributed the growth rate is reduced

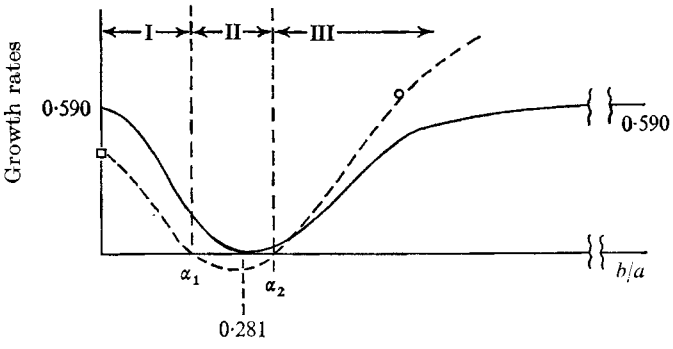

FIGURE 11. Perturbation theory growth rates. ——, von Kármán dispersion relation for asymmetric point vortex system; – – –, corresponding moderate-area system; ○, experiments VIII and IX; □, experiment X.

in regions I and II and increased in region III. These comments may resolve some problems and paradoxes raised by Wille (1960), who discusses mostly point vortex systems. He remarks (1960, p. 277) "On the whole the theory of vortex streets that comes under the heading *stability* is not yet satisfactory. One cannot easily understand the fact that the stability theory of first order describes the physical phenomenon in very good approximation, whereas further mathematical analysis always predicts instability, which means vortices cannot remain in a regular pattern." That is, if the Reynolds number is sufficiently high, the stabilizing finite-area effect can overcome the destabilizing second-order effects for the small region (α_1, α_2).

An obvious question can be posed. How does the slightly perturbed system evolve if $0 < b/a < 0{\cdot}281$? If the perturbation to the upper vortices is much smaller than b/a then both upper vortex regions will rise at a rate which decreases in time as they approach a 'stable band' around 0·281. The assumption of a decreasing rate is consistent with the observed lower growth rate of the collinear finite-area street described above and also with the Zabusky & Deem (1971) calculations, as illustrated in their figure 11 (*b*). It also accounts for the experimental observation shown by Wille (1960) in his figure 3. Here he presents a graph of the growth of a 'corrected' ratio $(b/a)_c$ versus distance behind a circular cylinder in water. The separation ratio begins at $(b/a)_c \simeq 0{\cdot}1$ and slowly grows to an asymptote $(b/a)_c = 0{\cdot}37$. The $(b/a)_c$ ratio then seems to oscillate around the asymptote (we see a slight decrease followed by an increase). According to § 6 above, we conclude that the vortex regions are oscillating in a quasi-stable region. We are not sure if $(b/a)_c = 0{\cdot}37$ is an estimate of the upper boundary of the 'stable band' or whether there is a systematic error in reducing the data to $(b/a)_c$. Furthermore, if the perturbation is sufficiently strong, the rising vortex regions will probably 'pass through' the stable band and undergo fusion as described in § 7.

At long times, systems with $b/a > 0{\cdot}281$ are unstable. Like-signed regions of vorticity attract and finally *fuse* (coalesce or 'condense'). For a collinear asymmetric street of strongly interacting vortices, we observed a linear growth phase

followed by a rapid *fission* of one vortex, due to the high-shear field produced by the nearest-neighbour opposite-signed vortex regions.

In the initial phases of evolution of an unstable laminar shear profile we have also observed an enhanced transport of vorticity across the dominant flow direction. This results from large-scale *convection* produced by vortex rotation (or 'nutation'). As the vortex street is forming, small opposite-signed ('secondary') vortices appear across the flow, as illustrated in figure 2. Smoke or other contaminant particles will also undergo convective transport. These results are in good agreement with those obtained by Zabusky & Deem and they are consistent with those of Abernathy & Kronauer.

For comparison with laboratory experiments, these late-time two-dimensional computational results should be considered qualitative and heuristic as *three-dimensional motions are probably generated during the breakdown and rapid rearrangement stages*. Vortex structures in the environment of a two-dimensional wind tunnel can have a longer lifetime than induced three-dimensional fluctuations. Thus our results qualitatively account for the vortex 'breakdown' and subsequent wavelength increase of vortex streets observed in 'two-dimensional' laboratory experiments by Taneda and others.

One of the authors (N.J.Z.) would like to acknowledge the support of the John Simon Guggenheim Memorial Foundation and Bell Laboratories, Inc. He also acknowledges the hospitality of Professor L. C. Woods and the Oxford University Mathematical Institute, and of Professor C. L. Pekeris and the Applied Mathematics Department of the Weizmann Institute, where parts of the manuscript were written. Both authors would like to thank Dr K. V. Roberts for his continued interest in this work, and David Howes for helpful assistance.

Appendix

Suppose we are given N sets of co-ordinates (x_i, y_i). From these co-ordinates the vorticity ζ is evaluated on a Cartesian mesh using an area-weighting technique (Harlow 1964; Amsden 1966). The stream function ψ in equation (4) is solved for by the Hockney technique (Christiansen & Hockney 1971). The fluid velocity, equation (3), is evaluated at mesh points by centred difference operations. To move the point vortices in their own velocity field a leapfrog time integration method is used so that a point vortex at time $t-\Delta t$ can be moved according to

$$\mathbf{r}(t+\Delta t) = \mathbf{r}(t-\Delta t) + \mathbf{u}(\mathbf{r}(t))\, 2\Delta t, \tag{A 1}$$

which approximates $d\mathbf{r}/dt = \mathbf{u}$. It is necessary to employ two sets of co-ordinates, one at even times $t+2n\Delta t$, one at odd times $t+(2n+1)\Delta t$. To evaluate the velocity $\mathbf{u}$ at the even position $\mathbf{r}(t)$ in order to move from the odd position $\mathbf{r}(t-\Delta t)$, the area-weighting technique is used again to interpolate from the velocity values known at the mesh points. In our experiments the VORTEX code computes a value of Δt that does not violate the Courant–Friedrichs–Lewy stability condition

$$\Delta t < \Delta x/|u_{\max}|, \tag{A 2}$$

Experiments	$\Delta E/E_0$	$\Delta\langle\zeta^2\rangle/\langle\zeta^2\rangle_0$	t_0
I	$1{\cdot}49\times10^{-2}$	$2{\cdot}62\times10$	8·75
II	$1{\cdot}47\times10^{-2}$	$5{\cdot}10\times10^{-2}$	8·75
III	$1{\cdot}49\times10^{-3}$	$8{\cdot}20\times10^{-2}$	8·75
IV	$1{\cdot}33\times10^{-3}$	$3{\cdot}80\times10^{-3}$	3·0
V	$2{\cdot}17\times10^{-3}$	$6{\cdot}37\times10^{-3}$	3·0
VI	$6{\cdot}20\times10^{-3}$	$2{\cdot}95\times10^{-1}$	23·5
VII	$1{\cdot}77\times10^{-3}$	$1{\cdot}63\times10^{-2}$	5·5
VIII	$1{\cdot}46\times10^{-3}$	$1{\cdot}26\times10^{-2}$	5·5
IX	$6{\cdot}11\times10^{-4}$	$5{\cdot}77\times10^{-3}$	7·5
X	$8{\cdot}93\times10^{-3}$	$2{\cdot}14\times10^{-1}$	16·5

TABLE 3. Temporal variations in energy and enstrophy for experiments I–X.

where $|u_{\max}|$ is the largest *particle* velocity and Δx is the constant mesh spacing ($\Delta x = \Delta y = 1{\cdot}0$).

During each numerical experiment we monitor the conservation of linear momentum and kinetic energy, as well as the mean-square vorticity, or 'enstrophy' by calculating

$$P_x = \sum_{i,j} u_x(i,j), \quad P_y = \sum_{i,j} u_y(i,j),$$

$$E = \sum_{i,j} u_x^2 + u_y^2,$$

$$\langle\zeta^2\rangle = \sum_{i,j} \zeta^2(i,j).$$

The incompressibility condition is identically satisfied for u_x and u_y at the mesh points at all times, such that a variation in P_x and P_y is due to computer rounding-off errors, which are of the order 10^{-5}, corresponding to 18 bits in a computer word. The variations in energy and enstrophy are due to the discretizations in time and space and reflect some of the inaccuracies of the model.

In table 3 we list the temporal variations in E and $\langle\zeta^2\rangle$. As a reference to figures 2, 4–8 and 10 we form the ratios $\Delta E/E_0$ and $\Delta\langle\zeta^2\rangle/\langle\zeta^2\rangle_0$, where E_0 and $\langle\zeta^2\rangle_0$ are the values at time $t = 0$ and ΔE and $\Delta\langle\zeta^2\rangle$ are the deviations from these values at the time t_0 indicated in the last frame.

The leapfrog scheme [equation (A 1)] will exhibit odd–even temporal numerical instabilities when applied to certain types of flows. The two alternating levels at times $(2n+1)\Delta t$ and $2n\Delta t$ will increasingly diverge from their average. To suppress this 'false' effect a smoothing procedure is applied at a certain frequency during the motion (Christiansen 1970).

REFERENCES

ABERNATHY, F. H. & KRONAUER, R. E. 1962 *J. Fluid Mech.* **13**, 1.

AMSDEN, A. A. 1966 The particle-in-cell method for the calculation of the dynamics of compressible fluids. *Los Alamos Sci. Rep.* LA-3466.

BASSETT, A. B. 1888 *A Treatise on Hydrodynamics*. Dover. (Corrected republication 1961.)

BEAVERS, G. S. & WILSON, T. A. 1970 Vortex growth in jets. *J. Fluid Mech.* **44**, 97.

CHRISTIANSEN, J. P. 1970 Vortex – a two-dimensional hydrodynamics simulation code. *UKAEA Culham Lab. Rep.* CLM-R106. H.M.S.O.

CHRISTIANSEN, J. P. 1971 Numerical simulation of hydrodynamics by the method of point vortices. *UKAEA Culham Rep.* CLM-P282. (To appear in *J. Comp. Phys.*)

CHRISTIANSEN, J. P. 1973 The non-linear dynamics of vortex flows by numerical methods. Ph.D. dissertation, University of Warwick.

CHRISTIANSEN, J. P. & HOCKNEY, R. W. 1971 DELSQPHI, a two-dimensional Poisson-solver program. *Comp. Phys. Comm.* **2**, 127.

CHRISTIANSEN, J. P. & ROBERTS, K. V. 1969 Rotational flows in a simple two-dimensional hydrodynamic fluid. *Proc. Comp. Phys. Conf., Culham Lab. July* 1969, vol. 2, paper 40.

DEEM, G. S., HARDIN, R. & ZABUSKY, N. J. 1971 Computer-generated film on instability and turbulence of two-dimensional incompressible fluids. Bell Laboratories (unpublished).

DURGIN, W. W. & CARLSON, S. K. F. 1971 *J. Fluid Mech.* **48**, 507.

GERRARD, J. H. 1967 *Proc. Roy. Soc.* A **261**, 137.

GRIFFIN, O. M. & VOTAW, C. W. 1972 *J. Fluid Mech.* **51**, 31.

HARLOW, F. H. 1964 The particle-in-cell computing method for fluid dynamics. *Methods in Computational Physics*, vol. 3, *Fundamental Methods in Hydrodynamics* (ed. B. Alder, S. Fernbach & N. Rotenberg), pp. 319–343. Academic.

HARLOW, F. H. 1970 Numerical methods for fluid mechanics. An annotated bibliography. *Los Alamos Sci. Rep.* LA-4281.

HARLOW, F. H. & FROMM, J. E. 1964 *Phys. Fluids*, **7**, 1147.

KOCHIN, N. E. 1939 On the instability of Kármán vortex streets (in Russian). *Dokl. Akad. Nauk. USSR.* **24**, 18–22.

KOCHIN, N. E., KIEBEL, I. A. & ROZE, N. V. 1964 *Theoretical Hydromechanics.* Interscience.

KOOPMAN, G. H. 1967 The vortex wake of vibrating cylinders at low Reynolds numbers. *J. Fluid Mech.* **28**, 501.

LAMB, H. 1932 *Hydrodynamics*, 6th edn. Cambridge University Press.

LEITH, C. E. 1968 *Phys. Fluids*, **11**, 671.

ROBERTS, K. V. & CHRISTIANSEN, J. P. 1972 Topics in computational fluid mechanics. *Comp. Phys. Comm.* **3** (suppl.), 14.

ROSENHEAD, L. 1929 The Kármán street of vortices in a channel of finite breadth. *Phil. Trans.* A **208**, 275.

ROSENHEAD, L. 1930 The spread of vorticity in the wake behind a cylinder. *Proc. Roy. Soc.* A **127**, 590.

SATO, H. & KURIKI, K. 1961 The mechanism of transition in the wake of a thin flat plate placed parallel to a uniform flow. *J. Fluid Mech.* **11**, 321.

TANEDA, S. 1959 Downstream development of wakes behind cylinders. *J. Phys. Soc. Japan*, **14**, 843.

TANEDA, S. 1965 Experimental investigation of vortex streets. *J. Phys. Soc. Japan*, **20**, 1714.

WILLE, R. 1960 Kárman vortex street. In *Advances in Applied Mechanics*, vol. 6 (ed. H. L. Dryden & Th. von Kármán), p. 273. Academic.

ZABUSKY, N. J. & DEEM, G. S. 1971 Dynamical evolution of two-dimensional unstable shear flows. *J. Fluid Mech.* **47**, 353.

ZDRAVKOVICH, M. M. 1968 Smoke observations of the wake of a group of three cylinders at low Reynolds number. *J. Fluid Mech.* **32**, 339.

ZDRAVKOVICH, M. M. 1969 Smoke observations of the formation of a Kármán vortex street. *J. Fluid Mech.* **37**, 491.